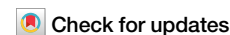


<https://doi.org/10.1038/s42003-024-07069-6>

# Proximal tubule cell maturation rate and function are controlled by PPAR $\alpha$ signaling in kidney organoids

Yoshiki Sahara<sup>1,2,3</sup>, Chie Fukui<sup>1</sup>, Yuki Kuniyoshi<sup>1,4</sup> & Minoru Takasato<sup>1,2,5</sup>  

Human pluripotent stem cell-derived kidney organoids are expected to be a useful tool for new drug discoveries, however, the immaturation of kidney organoids causes difficulties in recapitulating renal pharmacokinetics using organoids. Here, we performed time-course single-cell RNA sequencing of kidney organoids and revealed cell heterogeneity in the maturation rate of the proximal tubule. An unbiased analysis to identify upstream targets of genes that are expressed differentially between cells with low and high maturation rates revealed a higher activation of PPAR $\alpha$  signaling in rapidly maturing cells. Treatment with a combination of a PPAR $\alpha$  agonist and an RXR $\alpha$  agonist induced genes related to proximal tubule maturation and increased the capacity for protein uptake as well as the sensitivity to nephrotoxicity by cisplatin. This method to promote the maturation rate of proximal tubule cells has the potential to be utilized in microphysiological systems to recapitulate proximal tubule functions and to screen nephrotoxic drugs.

Recent progress in stem cell technology has enabled the generation of three-dimensional (3D) organ-like structures, so-called “Organoids”, from human pluripotent stem cells (hPSCs) for a variety of organs. We have previously generated kidney organoids from hPSCs using a 3D culture method *in vitro*<sup>1</sup>. This organoid technology is expected to be useful for regenerative medicine and drug discovery applications. In particular, regarding applications of kidney organoids for drug discovery, there are several reports on the analysis of regenerative mechanisms during proximal tubule injury using cisplatin<sup>2</sup> and a fibrosis model<sup>3</sup>. Additionally, several renal disease models, including those for autosomal dominant polycystic kidney disease (ADPKD)<sup>4,5</sup>, Alport syndrome<sup>6</sup>, and nephrotic syndrome<sup>7,8</sup>, have been developed using kidney organoids. Such a model that reflects human pathology is a useful tool for successful drug discovery, by which we could search for effective drug targets in human pathology or simulate drug responsiveness of human tissues *in vitro*.

Whereas kidney organoids from human induced pluripotent stem cells (hiPSCs) indeed have a capacity for certain renal functions such as protein reabsorption by proximal tubules and responsiveness to nephrotoxic substances, their maturity is not transcriptionally equivalent to adult kidneys but is similar to the first or second trimester of human embryonic kidneys<sup>1,2,9</sup>. As the immaturity of organoids causes imperfections in

mimicking the tissue morphology and functions of adult kidneys, it is necessary to grow kidney organoids to sufficient maturity to utilize them to model kidney diseases and to accurately evaluate the efficacy or toxicity of candidate drugs. However, current methods for the long-term culture of 3D tissues are suboptimal due to the lack of a proper vasculature system, which results in the failure of kidney organoid growth to larger sizes as well as to mature in function. To address this issue, a study showed glomerular vascularization and maturation of proximal tubules *in vitro* by culturing kidney organoids under flow on a microfluidic chip, and further studies are underway to achieve maturation *in vitro*<sup>10</sup>. Furthermore, as kidney organoids contain off-target cell populations<sup>11</sup>, long-term culture could negatively affect kidney organoids due to the proliferation of those cell populations<sup>12</sup>.

The developmental process of kidney organoids has been previously investigated using RNA-seq analyses, where variations in the developmental stage were observed between organoids as well as experiments<sup>13</sup>. In addition, whereas a single-cell RNA-seq analysis showed that a variety of renal cell populations developed within a single kidney organoid, it also revealed cell heterogeneity in the stage of nephrogenesis<sup>11,14</sup>. However, there have been no further studies investigating the mechanism(s) causing such cell heterogeneity within an organoid. Here, we aimed to identify novel factors that

<sup>1</sup>RIKEN Center for Biosystems Dynamics Research, Kobe, 650-0047, Japan. <sup>2</sup>Laboratory of Molecular Cell Biology and Development, Department of Animal Development and Physiology, Graduate School of Biostudies, Kyoto University, Kyoto, 606-8501, Japan. <sup>3</sup>Department of Drug Modality Development, Osaka Research Center for Drug Discovery, Otsuka Pharmaceutical Co. Ltd., Minoh, 562-0029, Japan. <sup>4</sup>Office of Bioinformatics, Department of Drug Discovery Strategy, Osaka Research Center for Drug Discovery, Otsuka Pharmaceutical Co. Ltd., Minoh, 562-0029, Japan. <sup>5</sup>Department of Development and Regeneration, Graduate School of Medicine, Osaka University, Suita, 565-0871, Japan. ✉e-mail: [minoru.takasato@riken.jp](mailto:minoru.takasato@riken.jp)

promote the maturation rate of cells within kidney organoids without prolonging the period of cell culture. As for the strategy to search for such factors, we focused on cell heterogeneity and performed a time-course single-cell RNA-seq analysis of kidney organoids to detect genes that are differentially expressed between fast- and slow-maturing cells.

## Results

### Clustering and identification of cell types in kidney organoids

First, to reveal the dynamics of cell heterogeneity within human kidney organoids, time-course single-cell RNA sequencing (scRNA-seq) was performed using organoids at 5 timepoints, days 15, 19, 23, 27 and 31 of differentiation (Fig. 1a, b), during which time each segment of the nephron developed into a mature state. Uniform Manifold Approximation and Projection (UMAP) analysis, a dimension reduction method, of the integrated scRNA-seq dataset of kidney organoids from day 15 to day 31 detected 17 different cell clusters (Fig. 1c). Those clusters were annotated using known marker genes and were categorized as various cell types of the nephron, including nephron progenitor cell (NPC/PTA; CL2, 12), glomerulus (CL0, 1, 7, 13), proximal tubule (CL4), distal tubule (CL5) as well as off-target lineages (CL6: cartilage, 11; neuron\_1, 14; muscle, 15; neuron\_2) (Fig. 1e). UMAP analysis also showed the developmental trajectory of cells in kidney organoids where relatively uniform cell clusters at day 15 dynamically differentiated into each segment of the nephron and renal stroma (Fig. 1d). These results demonstrated that the time-course scRNA-seq analysis of kidney organoids successfully displayed the transcriptional changes of developing nephrons at a single-cell level.

To identify cell types that could not be classified by the parameters when using all samples, sub-clustering was performed for each cluster of NPC/PTA (CL2, 12, 13), tubules (CL4, 5, 9) and glomeruli (CL0, 1, 7). Sub-clustering was performed for each cluster of NPC/PTA clusters, and the results of the sub-clustering showed that, apart from the NPC/PTA clusters (*EYA1*, *CITED1*, *ITGA8*), the clusters of Renal vesicle (RV) (*CCND1*, *LHX1*, *JAG1*) and S-shaped body (SSB) seen during development clusters (proximal: *OLFM3*, distal: *POU3F3*, *IRX1*), could be classified into six sub-clusters (Supplementary Fig. 1a–c).

Clusters of tubules (CL4, 5, 9) were sub-clustered using the distal tubule lineage distal SSB (dSSB) and distal tubule markers (*POU3F3*, *IRX1*, *MAL*, *MECOM*, *SLC12A1*, *CLCNKB*), and the proximal tubule lineage medial SSB (mSSB) and proximal tubule sub-clustering with markers (*CDH6*, *HNF4A*, *SLC3A1*, *CUBN*, *LRP2*) allowed clusters that were “Early tubules” in the first clustering analysis to be classified as mSSB or dSSB. Some cells that were determined to be tubule clusters also contained cells from the RV and cells from podocytes (Supplementary Fig. 1d–f). Sub-clustering using clusters of glomeruli (CL0, 1, 7) showed that it was possible to classify the glomeruli into several clusters with high expression of *OLFM3*, which is expressed early in glomerulogenesis, and with different expression levels of podocyte markers (*PODXL*, *NPHS1*, *PTPRO*), representing different maturation levels within podocytes (Supplementary Fig. 1g–i).

### Pseudotime cell trajectory of maturing cells during nephron development

Next, to analyze the cell heterogeneity in the maturation rate during nephron development, we extracted data of cells in nephric lineages and performed pseudotime cell trajectory analysis using Monocle 2 (Fig. 2a–e). By aligning dots that resemble the transcriptional profile of single cells in three dimensions along with the gene expression changes, the trajectory was created with four branches and composed of seven cell states. The trajectory plots showed that cells first started at the NPC/PTA state and differentiated into podocytes or tubular lineage, after which the tubular lineage branched into proximal and distal tubules. A heatmap showing the gene expression dynamics along the pseudotime from branch point 1 indicated that the expression of NPC/PTA marker genes (*SIX2*, *CCND1*, *TMEM100*, *ITGA8*, *EYA1*) was higher at the root, and immature podocyte marker genes (*SIX1* and *OLFM3*)<sup>15</sup> were expressed in the trajectory toward podocytes, followed

by the expression of mature podocyte marker genes (*NPHS1*, *NPHS2*, *PTPRO* and *PODXL*). On the other hand, in the trajectory toward tubules, markers for medio-distal RV and SSB (*LHX1*, *JAG1*) were expressed first, then the distal tubule markers and the proximal tubule markers followed in the latter half of the pseudotime (Fig. 2f). In the heatmap showing branch point 2 onward, cells differentiated into either the proximal tubule (*ABCBI*, *HNF4A*, *SLC3A1*, *LRP2*, *CUBN*) or the distal tubule (*MECOM*, *CLCNKB*, *MAL*, *SLC12A1*) (Fig. 2g). Notably, lineage commitment of PTA cells to distal tubules occurred earlier than that to proximal tubules, which is consistent with a previous study about human nephron development<sup>16</sup>. This pseudotime cell trajectory study demonstrates that the dataset of time-course scRNA-seq is capable of displaying the gene expression dynamics along the process of human nephrogenesis.

### DEG analysis by comparing cell populations with different maturation rates

Focusing on proximal tubule maturation, the data of cells annotated as proximal tubule status was re-analyzed by monocle analysis. We used a combination of cells annotated as PT series (RV, medial SSB, PT1 and PT2) in the Seurat sub-clustering of tubule clusters (CL4, 5, 9) (Supplementary Fig. 1f) and cells annotated as PT state in the monocle cell trajectories (Fig. 2b). Using scRNA-seq data of these cells, we created a pseudotime cell trajectory (0–20) in which proximal tubule cells were arranged on a trajectory without branching (Fig. 2h, i). Using this pseudotime, we created a violin plot to show the separate cell trajectory for each day (Fig. 2j). In the violin plot, almost all cells from sampling day 19 were plotted in the early pseudotime (0–5), cells from day 23 emerged in the late pseudotime (10–20) and cells from day 31 remained rarely in the early pseudotime (0–5) (Fig. 2j). As expected, the cells from each sampling date were distributed across a wide range of pseudotime, demonstrating cell heterogeneity in the maturation rate of proximal tubule cells (Fig. 2h–j). We identified a group of genes that were highly expressed in the later stages of pseudotime, as shown in a FeaturePlot (Fig. 2k, l). These genes were then used as markers of proximal tubule maturation in subsequent experiments.

Using this pseudotime cell trajectory of proximal tubule maturation, we compared cells from different sampling days at the same maturity level to extract a set of genes related to maturation rate. Analyzing a certain maturity level, cells from a shorter differentiation period can be presumed to have a faster maturation rate. In this study, we set a certain maturity range, pseudotime 8–11, as a maturation stage, and compared cells from day 23 (blue bracket “a” in Fig. 2j, cells with faster maturation rate) and day 27 (red bracket “b” in Fig. 2j, cells with slower maturation rate) in that range to obtain differentially expressed genes (DEGs) (Fig. 2j).

To exclude genes whose expression levels increased in a time-dependent manner, we compared gene expression levels in d19 and d31 cells and excluded genes whose expression was high in d19 from maturation-related genes. Such DEGs are expected to be involved in the regulation of proximal tubule maturation rate, and 232 genes were identified (Table 1, Supplementary Data 1). To identify upstream regulators of those DEGs, we performed an upstream regulator analysis using Ingenuity® Pathway Analysis (IPA) (Table 2). As a result, the majority of candidate molecules regulating the DEGs were associated with pathways activated by nuclear receptors. Such molecules were *PPARA*, *HNF4A*, and *PPARA* agonists, including pirinixic acid, bezafibrate, mono-(2-ethylhexyl) phthalate and fenofibrate (Table 2). These results suggest that pathways associated with *PPARA* and *HNF4A* are activated in a group of proximal tubule cells with a faster maturation rate to boost the maturation in kidney organoids.

### Induction of maturation markers in proximal tubular cells by activating the PPARα pathway

Since scRNA-seq analysis showed DEGs that are expressed at high levels in faster maturing proximal tubule cells in kidney organoids as downstream targets of the *PPARA* pathway, we tested whether agonists of *PPARA* in combination with agonists of *RXRα*, which forms a heterodimer to

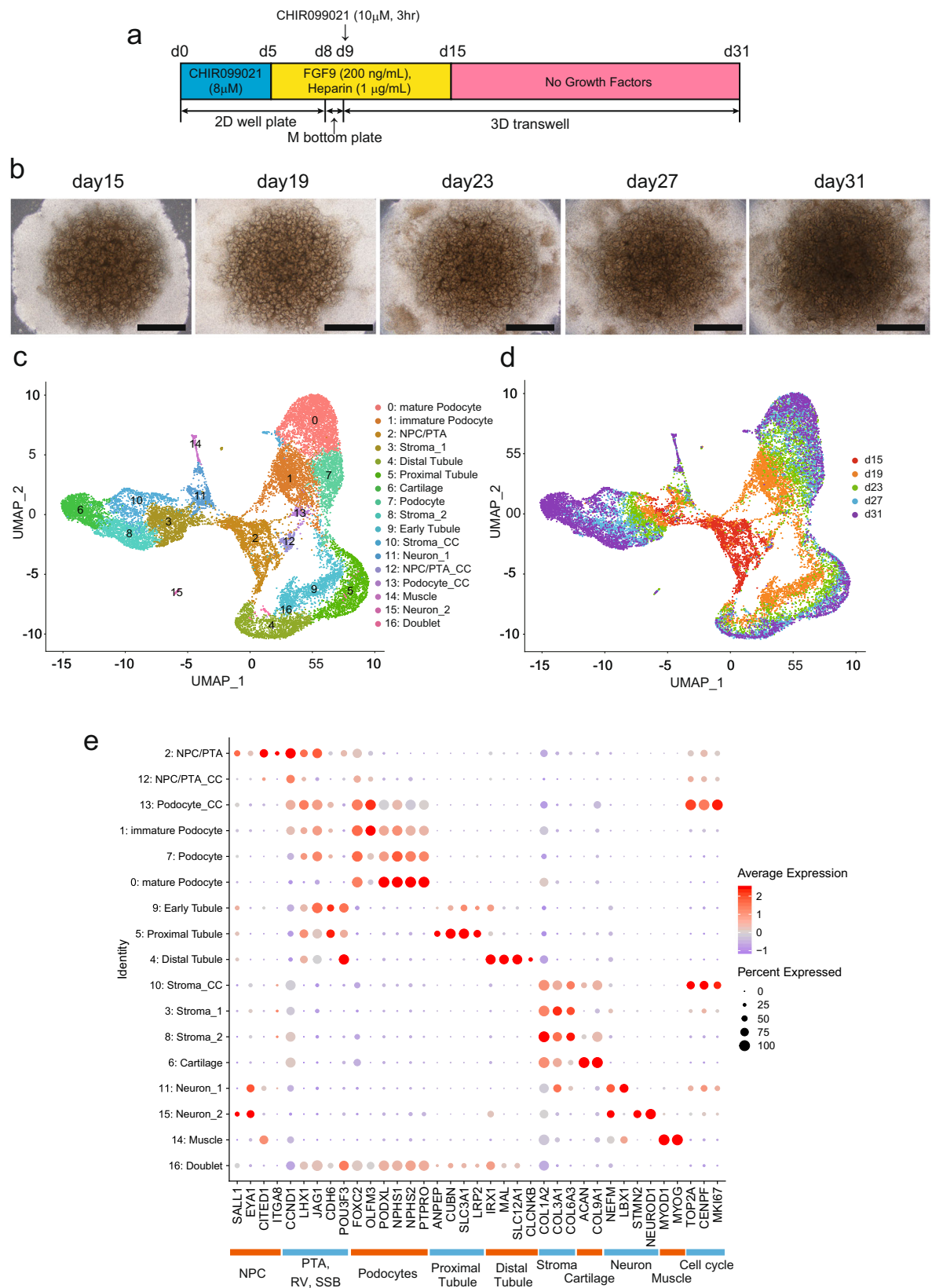


**Fig. 1 | Cell heterogeneity in kidney organoids differentiated from human iPSCs.** **a** Scheme of the induction protocol of kidney organoids from iPSCs. **b** Phase contrast images of kidney organoids at days 15, 19, 23, 27 and 31. Scale bars, 1 mm.

**c, d** Uniform Manifold Approximation and Projection (UMAP) plot of kidney organoids colored by clusters (**c**) and differentiation day (**d**). **e** Dotplot of all clusters with known kidney marker genes.

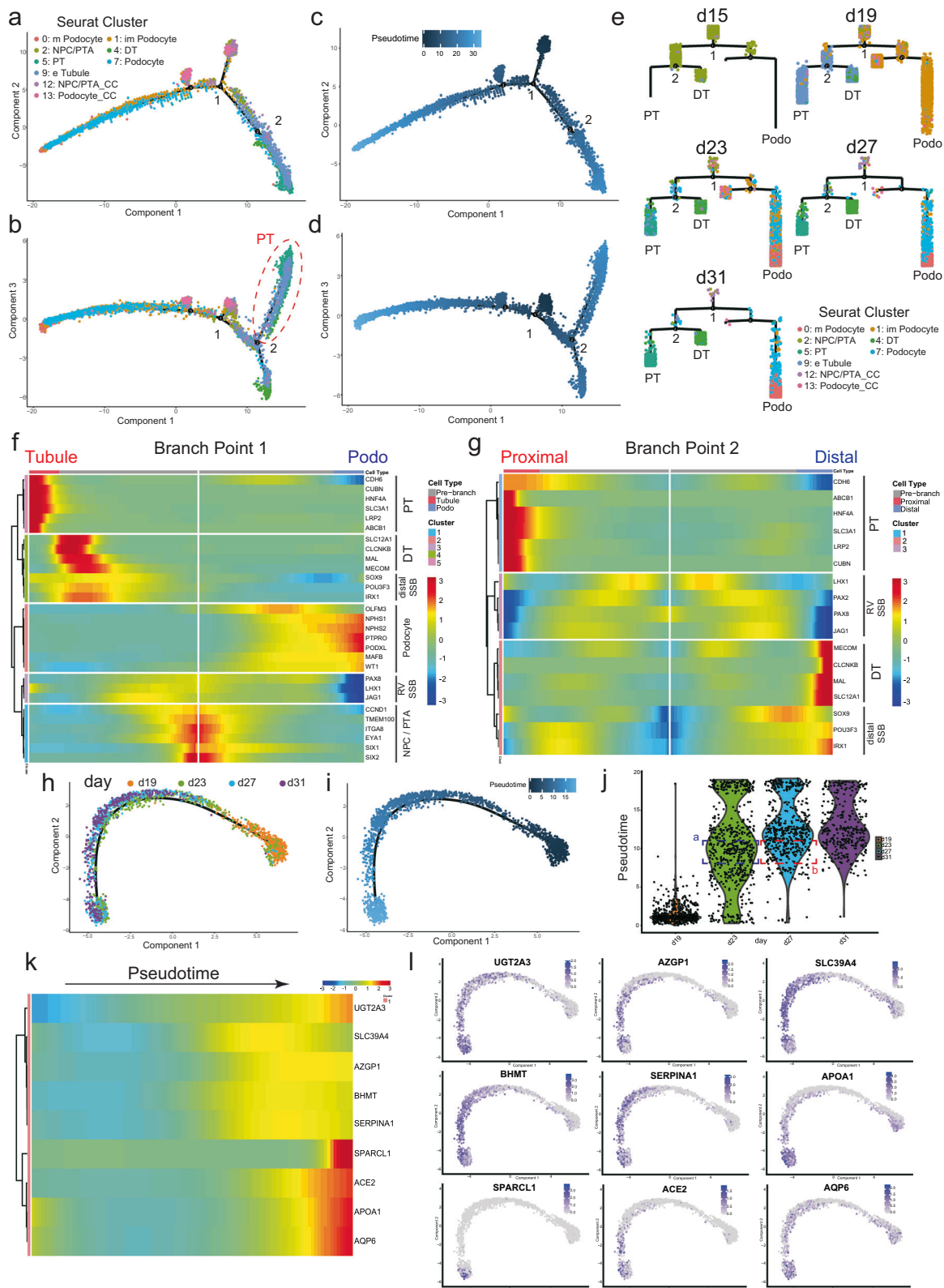


**Fig. 2 | Pseudotime cell trajectories of kidney lineage cells in kidney organoids.** a–d Pseudotime cell trajectory of component 1 against component 2 colored by Seurat clusters (a) and pseudotime (c). Pseudotime cell trajectory of component 1 against component 3 colored by Seurat clusters (b) and pseudotime (d). 1 and 2 indicate the branch points. The red dashed line indicates the proximal tubule state (PT). e Plot complex cell trajectory of each time point colored by Seurat clusters. 1 and 2 indicate the branch points. f, g Branched heatmap for known marker genes of

kidney development at branch point 1 (f) and branch point 2 (g). h, i Pseudotime cell trajectory of proximal tubule lineage cells in kidney organoids colored by day (h) and colored by pseudotime (i). j Violin plot of cells from proximal tubule lineage cells against pseudotime at each time point. Blue and red brackets indicate proximal tubule cells with pseudotime 8–11 at day 23 and day 27, respectively. k, l Pseudotime heatmap of genes altered in the late stage of pseudotime cell trajectory using proximal tubule lineage cells (k) and feature plots of those genes (l).

transcriptionally activate the expression of target genes, could upregulate those DEGs and boost the maturation of proximal tubules by adding them to the culture medium for kidney organoids. As shown by sub-clustering analysis (Supplementary Fig. 1c), it was observed that proximal-distal patterning of nephron development had been already initiated at day 15 of organoids, therefore, we tested agonists to organoids from day 15 and harvested organoids at day 23 followed by the purification of proximal tubule cells using magnetic cell sorting (MACS) (Fig. 3a). Expression levels of downstream genes of PPAR $\alpha$  in purified proximal tubule cells were upregulated in the group treated with the combination of PPAR $\alpha$  and RXR $\alpha$  agonists (PPAR $\alpha$  agonists-treated group), confirming the successful activation of the PPAR $\alpha$  pathway in proximal tubule cells (Fig. 3b). In addition, proximal tubule markers (Fig. 3d) and proximal tubule maturation markers (Fig. 3c–e) were significantly elevated in the agonist-treated group. On the other hand, the PPAR $\alpha$  antagonist GW6471 and the RXR $\alpha$  antagonist

HX531 reduced the expression of proximal tubule maturation markers (Supplementary Fig. 2). The proximal tubule marker, megalin (gene *LRP2*), was quantitatively analyzed via immunofluorescence staining. The fluorescence intensity per unit area of megalin expression was measured over time in both the control and PPAR $\alpha$  agonists-treated groups. We observed that megalin fluorescence intensity increased over time, with this increase tending to be higher in the PPAR $\alpha$  agonists-treated group, and reaching significance on day 26 (Fig. 3f, g). These findings suggest that the PPAR $\alpha$  agonist not only upregulates *LRP2* expression but also enhances megalin protein expression. However, immunostaining images of whole kidney organoids did not reveal obvious changes in the structure of individual nephron segments between the two groups (Supplementary Fig. 3b, c). Further, there was no significant difference in the ratio of proximal tubule cell population (LTL-FITC-positive) within kidney organoids between two groups (Supplementary Fig. 3d, e), indicating that activation of the PPAR $\alpha$  pathway did not affect early nephron development for its fate decision. These results demonstrate that the maturation markers of proximal tubules in kidney organoids are regulated via the PPAR $\alpha$  pathway.

**Table 1 | Top 20 out of 232 differentially expressed genes detected to be expressed higher in day 23**

Gene	p-value	padj	Fold change
APOA1	2.98E-32	7.58E-28	1.916
SLC51B	1.05E-39	2.68E-35	1.820
SLC13A1	4.62E-28	1.17E-23	1.721
TUBB4B	5.32E-190	1.35E-185	1.702
S100A1	5.19E-33	1.32E-28	1.678
AGT	5.07E-30	1.29E-25	1.657
SLC39A4	3.10E-38	7.89E-34	1.596
HAO2	1.71E-18	4.35E-14	1.570
RGN	9.14E-23	2.32E-18	1.558
ALDH1A1	1.24E-107	3.15E-103	1.549
PSAT1	9.91E-20	2.52E-15	1.527
NIT2	2.27E-59	5.76E-55	1.519
FABP1	2.90E-15	7.36E-11	1.514
ETFB	3.07E-55	7.80E-51	1.512
PPP1R16A	4.93E-33	1.25E-28	1.507
APOE	0.00E+00	0.00E+00	1.490
ACSM2A	1.75E-20	4.45E-16	1.471
TPD52L1	1.03E-20	2.62E-16	1.457
SLC34A1	6.74E-14	1.71E-09	1.455
GPX3	1.47E-25	3.74E-21	1.454

The top 20 are ranked based on fold change.

### Comparison of proximal tubule cell maturity between kidney organoids and human kidney tissue

To compare the level of maturity of proximal tubule cells in kidney organoids against human kidneys, we performed scRNA-seq on the control and PPAR $\alpha$  agonists-treated group at day 23. First, we integrated the data from day 23 of the kidney organoids with the data of human fetal kidneys from Kidney Cell Atlas (KCA)<sup>17</sup> and annotated the 9 clusters based on the fetal annotations and known marker genes (Fig. 4a–c). No significant changes in the proportion of proximal tubules within the nephrons were observed between the control group and the PPAR $\alpha$  agonists-treated group (Supplementary Fig. 4b). At day 23, the expression of off-target marker genes (cartilage: *ACAN*, neuron: *STMN2*, *LBX1*, muscle: *MYOG*) was scarcely observed in both the control group and PPAR $\alpha$  agonists-treated group (Supplementary Fig. 4e).

Within the proximal tubule cluster (CL4), a violin plot of the maturation markers (Fig. 2g) confirmed a higher proportion of cells expressing these markers in the PPAR $\alpha$  agonists-treated group (Fig. 4d). As expected, the expression of these maturation markers was not upregulated by the PPAR $\alpha$  agonist in the podocyte cluster (CL0) or the distal tubule cluster (CL5) (Supplementary Fig. 4c, d).

To ascertain the level of maturity of these proximal tubule cells compared to fetal and adult kidneys, we obtained DEGs between mSSB and proximal tubule cells in fetal kidneys; performed PCA on KCA Fetal mSSB, PT, and KCA Child PT to create a pseudotime of maturity; and compared the proximal tubule cells of the organoids with the samples of fetal<sup>17</sup>, child<sup>17</sup> and adult<sup>18</sup>. As a result, the PPAR $\alpha$  agonists-treated group slightly sifted to the higher pseudotime position that that in the control group. Of note, the

**Table 2 | Upstream regulator analysis using IPA**

Upstream regulator	Molecule type	Predicted activation state	Activation z-score	p-value of overlap
PPARA	Ligand-dependent nuclear receptor	Activated	2.626	1.97E-12
HNF4A	Transcription regulator	Activated	2.598	2.53E-11
Pirixinic acid	Chemical toxicant	Activated	3.142	4.25E-11
Mono-(2-ethylhexyl)phthalate	Chemical toxicant	Activated	3.357	1.84E-10
Bezafibrate	Chemical drug	Activated	2.553	4.79E-09
Fenofibrate	Chemical drug	Activated	2.385	1.40E-07
Gemfibrozil	Chemical drug	Activated	2.809	7.21E-07
LHX1	Transcription regulator	Activated	2.395	1.39E-06
TP53	Transcription regulator	Activated	2.517	1.92E-06
CAB39L	Kinase	Activated	2.449	2.44E-06

The top 10 predicted activators are ranked based on the p-value of overlap.

PPARA peroxisome proliferator-activated receptor alpha, HNF4A hepatocyte nuclear factor 4-alpha, LHX1 LIM Homeobox 1.

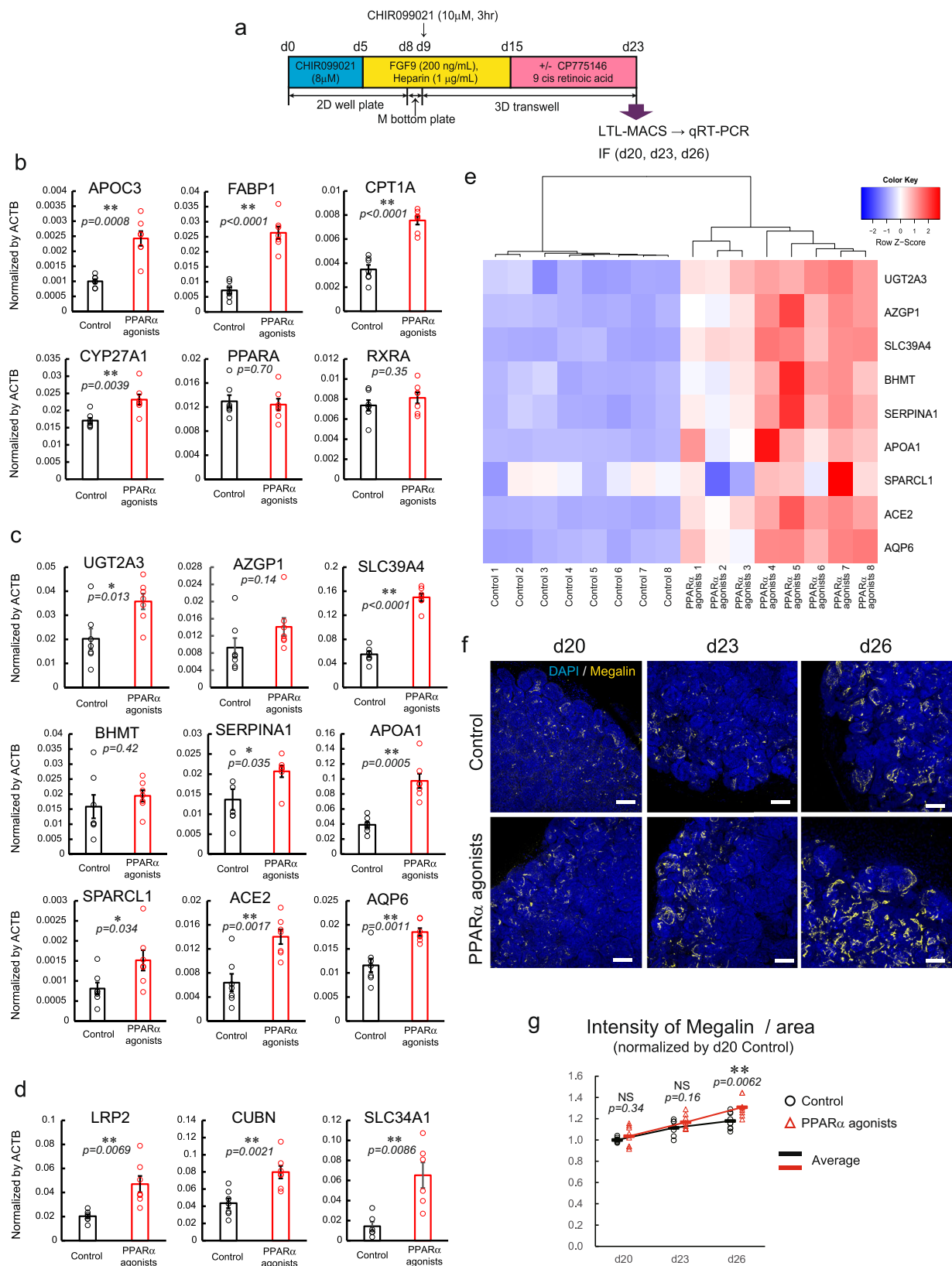


**Fig. 3 | Activation of the PPAR $\alpha$  pathway increases the expression of maturation markers in proximal tubule cells sorted by LTL-MACS from kidney organoids.** **a** Scheme of the induction protocol of kidney organoids from hiPSCs treated with PPAR $\alpha$  agonists. **b–d** Gene expression levels of downstream genes of the PPAR $\alpha$  pathway and gene expression levels of PPAR $\alpha$  and RXRA (**b**), maturation markers (**c**) and proximal tubule markers (**d**) in proximal tubule cells of day 23; means  $\pm$  SE,  $n = 7–8$  experiments. **e** Heatmap showing the expression levels of maturation marker genes from each sample treatment with or without PPAR $\alpha$  agonists.

Columns indicate data for each sample from positive fractions of LTL-MACS-sorted kidney organoids treated with vehicle or PPAR $\alpha$  agonists. **f** Immunostaining of megalin in kidney organoids at day 20, 23, and 26 treatments with vehicle (Control) or PPAR $\alpha$  agonists. Megalin: Yellow, DAPI: Blue, Scale bars, 100  $\mu$ m. **g** Dotplots of the intensity of megalin per area in the control group and PPAR $\alpha$  agonists-treated group at days 20, 23, and 26 of kidney organoids normalized by the control group at day 20; means  $\pm$  SE,  $n = 7$  experiments. Statistical significance was determined by unpaired two-tailed *t*-test (\* $p < 0.05$ , \*\* $p < 0.01$ ).

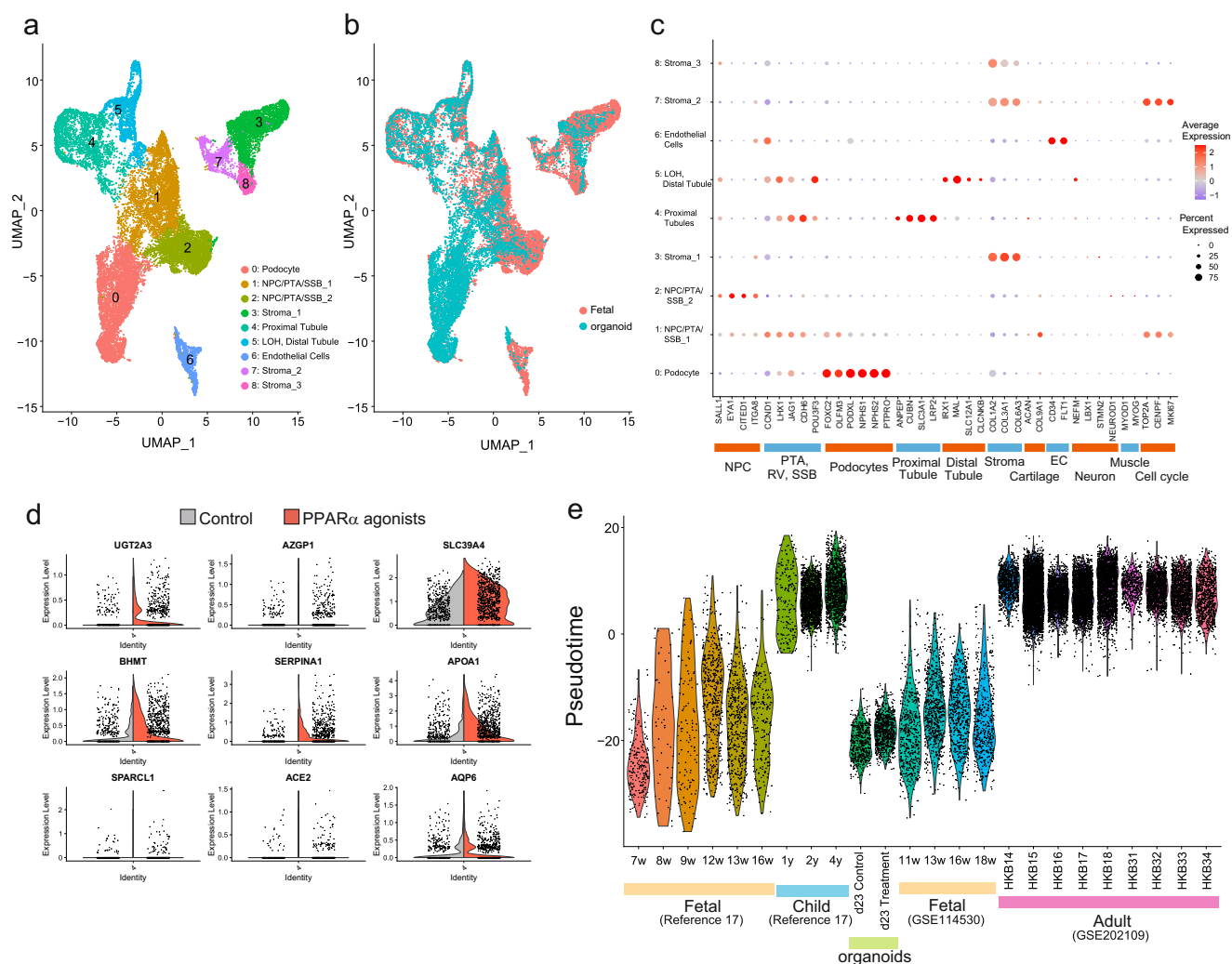


**Fig. 4 | Comparison of maturity levels of proximal tubule cells within fetal, child, and adult kidneys and kidney organoids by using scRNA-seq. a, b** UMAP plot of kidney organoids and fetal kidneys colored by clusters (a) and origin of data (b). **c** Dotplot of all clusters with known kidney marker genes. **d** Violin plot of CL4 in

kidney organoids with proximal tubule maturation markers. Gray: control group, Red: PPARα agonists-treated group. **e** Violin plot of pseudotime of proximal tubule maturation in KCA fetal, KCA child, organoids, fetal kidneys, and adult kidneys.

maturity of proximal tubule cells in kidney organoids stayed within the range of the maturity as that in human fetal kidneys (Fig. 4e).

### Functional maturation of proximal tubules by activating the PPARα pathway

One of the main functions of proximal tubules is the reabsorption of proteins excreted in the urine. In proximal tubules of a rat fetus, the number of intracellular endosomes increases with development<sup>19</sup>, and vesicles larger than 0.5 μm<sup>2</sup> are formed in the late stage of development<sup>20</sup>. Based on those previous studies, we evaluated the functional maturation of proximal tubules in the PPARα agonists-treated group by quantifying the number of endosomes per proximal tubule cell area using transmission electron microscopy (TEM) (Fig. 5a–c). As a result, the number of endosomes per cell area significantly increased, and the number of large endosomes (more than 0.5 μm<sup>2</sup>) was higher in the PPARα agonists-treated group (Fig. 5d, e). In addition, the reabsorption function of proximal tubule cells was assessed by a 10 kDa dextran uptake for 24 h and displayed an increased uptake of dextran per proximal tubule area in the PPARα agonists-treated group (Fig. 5f, g). This uptake was significantly reduced in the PPARα antagonist-treated group (Supplementary Fig. 5). In summary, the reabsorption function of proximal tubules in kidney organoids was matured by activation of the PPARα pathway.

### Cisplatin-induced nephrotoxicity assay using matured proximal tubules in kidney organoids

Since the generation of kidney organoids was first reported, they have been expected to be utilized for nephrotoxicity screening. Thus, we assessed the feasibility of mature kidney organoids for nephrotoxicity tests using cisplatin, an anti-cancer drug that causes damage to proximal tubule cells. As previously reported, cisplatin causes cell death in proximal tubules of kidney organoids in a dose-dependent manner, and a low dosage of cisplatin, such as 5 μM, can minimally affect the organoids<sup>21</sup>. Furthermore, treating kidney organoids with Cisplatin 5 μM for 1 day results in an increase in γH2AX-positive cells in the proximal tubules, indicating cellular damage caused by cisplatin<sup>22</sup>. Therefore, cisplatin treatment was initiated from day 23, when the expression of maturation markers significantly increased, and carried out for 1 day until day 24 and for 6 days until day 29 at a low concentration (5 μM)<sup>21,22</sup> (Fig. 6a). As a result, in the 1-day treatment of cisplatin, the number of γH2AX-positive cells in the proximal tubules significantly increased with cisplatin treatment in both the control group and PPARα agonists-treated group. In the 6-day treatment of cisplatin, γH2AX increase in the PPARα agonists-treated group was substantially higher than that in the control (Fig. 6b, c, Supplementary Fig. 6). Flow cytometry analysis after 6 days of cisplatin treatment showed the percentage of the proximal tubule cell population was unchanged in the control group (*p* = 0.75), but

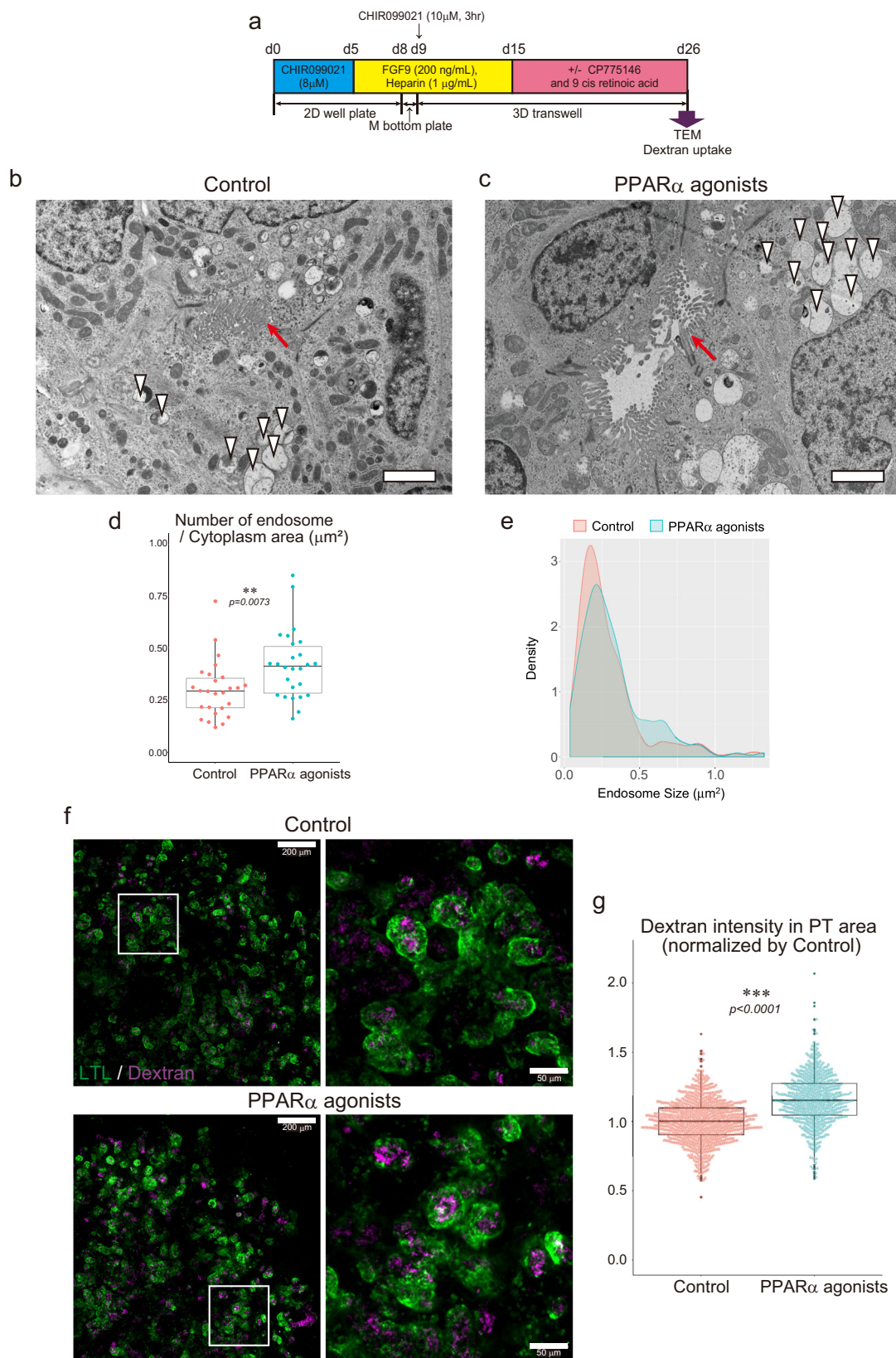


**Fig. 5 | Functional maturation of proximal tubules by activation of the PPARα pathway.** **a** Scheme of the induction protocol of kidney organoids from hiPSCs treated with PPARα agonists for TEM and dextran uptake assay. **b, c** TEM images from the control (**b**) and the PPARα agonists-treated group (**c**). White arrowheads indicate endosomes; Red arrows indicate brush borders. Scale bar, 2 μm. **d, e** Number of endosomes per 1 μm<sup>2</sup> of cytoplasm in the proximal tubule cell (**d**), and density plot for endosome size in proximal tubule cells (**e**) from TEM image treated with control or PPARα agonists-treated group;  $n = 26$  cells.

**f** Immunostaining of pHrodo™ Red Dextran uptake into kidney organoids in control and in PPARα agonists-treated group. Right panels represent magnifying images of each condition. LTL: Green, pHrodo™ Red Dextran 10,000 MW: Magenta, scale bars: 200 μm and 50 μm. **g** Dotplots of intensity of dextran in PT areas normalized by control group;  $n = 746$  (from 5 organoids) in control group,  $n = 652$  (from 5 organoids) in PPARα agonists-treated group. Statistical significance was determined by unpaired two-tailed *t*-test (\*\* $p < 0.01$ , \*\*\* $p < 0.001$ ).

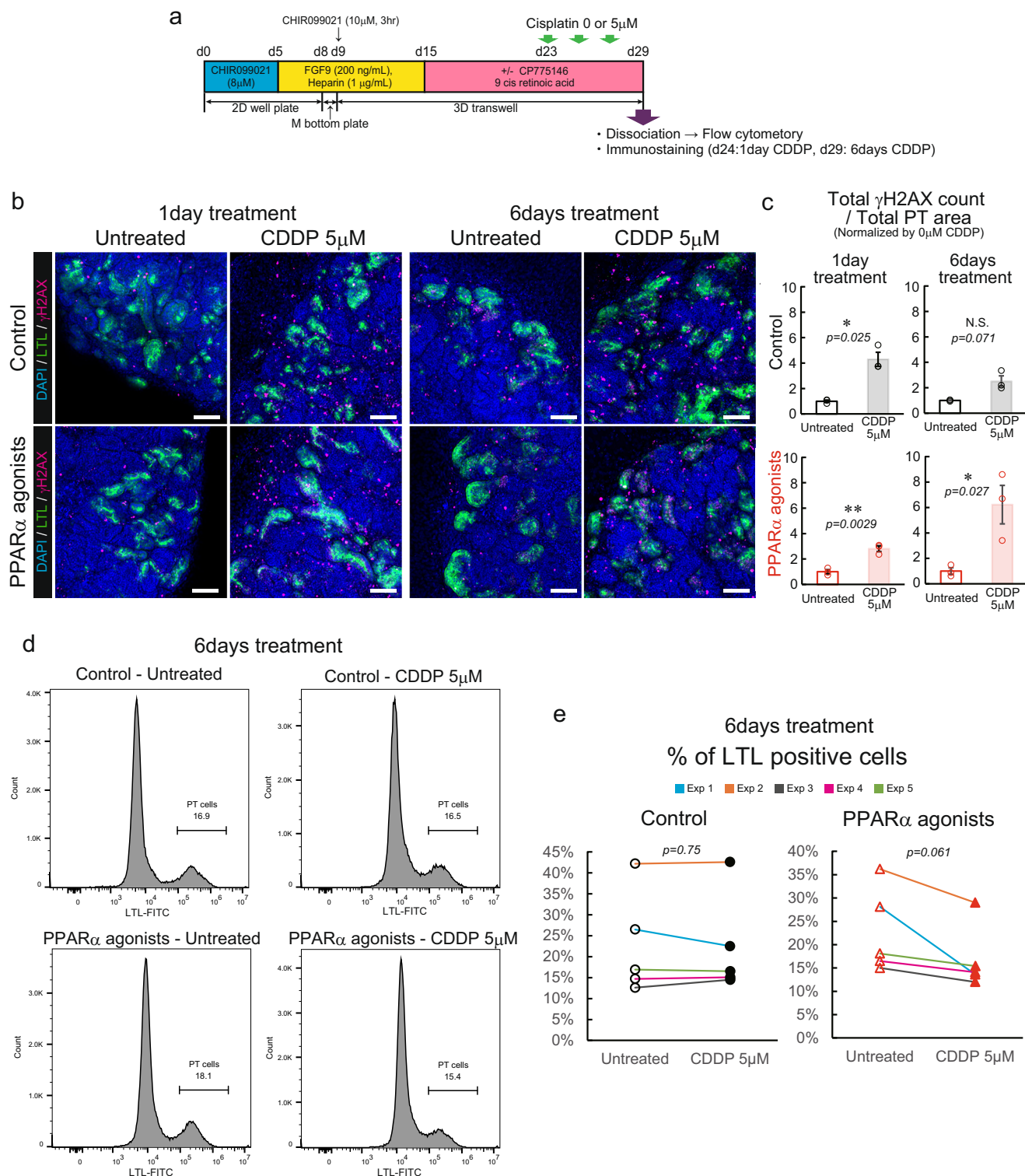


**Fig. 6 | Cisplatin-induced nephrotoxicity assay using mature proximal tubules in kidney organoids.** **a** Scheme of the induction protocol of kidney organoids from hiPSCs treated with PPAR $\alpha$  agonists for cisplatin-induced nephrotoxicity assay. **b** Representative immunostaining images of cisplatin treatment for 1 day and 6 days in the control and PPAR $\alpha$  agonists-treated groups. Blue: DAPI, Green: LTL, Magenta:  $\gamma$ H2AX. Scale bars, 100  $\mu$ m. **c** Quantification of total  $\gamma$ H2AX counts in the PT area within kidney organoids after cisplatin treatment for 1 day and 6 days in the control and PPAR $\alpha$  agonists-treated groups. The Y-axes were normalized to the average value of the cisplatin-untreated group, which was set as 1. Images of the entire kidney organoid were captured, and the staining was performed using three

organoids per group. Data are presented as means  $\pm$  SE,  $n = 3$  experiments. Statistical significance was determined by unpaired two-tailed  $t$ -test ( $*p < 0.05$ ,  $**p < 0.01$ ). **d** Representative histograms of LTL-FITC in the control group with untreated (upper left), with CDDP 5  $\mu$ M (upper right), or in PPAR $\alpha$  agonists-treated group with untreated (lower left), with CDDP 5  $\mu$ M (lower right). The numbers represent the percentage of LTL-FITC positive cells (PT cells). **e** Percentage of LTL-positive cells in the control group and PPAR $\alpha$  agonists-treated group before and after treatment with CDDP 5  $\mu$ M for 6 days. The color of the lines indicates the same experimental run;  $n = 5$  experiments. Statistical significance was determined by paired  $t$ -test.

considerably decreased in the PPAR $\alpha$  agonists-treated group ( $p = 0.06$ ) (Fig. 6d, e). These results suggest that activating PPAR $\alpha$  signaling within kidney organoids could potentially improve the susceptibility of proximal tubule cells to nephrotoxicity caused by low-dose cisplatin.

## Discussion

In this study, to confirm the heterogeneity of proximal tubule cells within the kidney organoids, we sampled the organoids at four-day intervals from day 15 to day 31 after differentiation induction. In kidney organoid differentiation, day 15 is the stage when the proximal-distal patterning of the nephron is established, as evidenced by the presence of podocyte-specific markers and early nephron structures. While the original protocol specifies a culture period until day 26–27, we extended the culture to day 31 to allow for further maturation.

PPAR $\alpha$  is a nuclear receptor that regulates the expression of a group of genes related to lipid metabolism by forming heterodimers with the retinoic acid X receptor RXR and binding to a specific cis-element, the PPAR $\alpha$  ligand response sequence PPRE (DR-1)<sup>23</sup>. In humans, PPAR $\alpha$  is mainly expressed in tissues with high fatty acid catabolism (adipose tissue, liver, heart, muscle and renal cortex)<sup>23</sup>, and in the kidney, it is abundant in the proximal tubules and the thick ascending legs of medulla, and less so in mesangial cells<sup>24</sup>. In addition, fatty acid oxidation (FAO) and mitochondrial respiration play an important role in proximal tubule function because of the high abundance of mitochondria in proximal tubule cells<sup>25</sup>. Recent studies have suggested there is a shift in metabolism from glycolysis toward FAO during human kidney development, and treatment with butyrate, one of the short-chain fatty acids (SCFAs), elevated CPT1 expression and proximal tubule marker expression in human iPSC-derived kidney organoids<sup>26</sup>. Thus, the acquisition of a metabolic system by FAO is thought to be important for the function of mature proximal tubules. This proximal tubule maturation by butyrate treatment supports the results of this study that activation of the PPAR $\alpha$  pathway is involved in proximal tubule maturation. A recent study<sup>27</sup> demonstrated a correlation between proximal tubule differentiation and metabolic changes in human kidney organoids. In fibrosis model mice, a reduction in oxidative phosphorylation and lipid metabolism compared to that in normal mice has been observed, suggesting that these factors are critical for maintaining proximal tubules. This study showed that culturing human kidney organoids in oxidative phosphorylation medium for 4 days increased the number of proximal tubules compared to culturing in glycolytic medium. However, this study did not investigate the effects of treatment with a PPAR $\alpha$  agonist alone on proximal tubules in human kidney organoid cultures. Our research demonstrated that treatment of human kidney organoids with a PPAR $\alpha$  agonist after the completion of nephrogenesis patterning resulted in increased expression of maturation marker genes (Supplementary Figs. 3b–e, 4b, Fig. 4d). Therefore, the increased expression levels of maturation marker genes in proximal tubules following PPAR $\alpha$  agonist treatment are likely due to accelerated maturation of proximal tubule cells rather than promoting new differentiation into proximal tubules. This is also suggested by the fact that *PPARA* expression is more abundant in proximal tubules and the thick ascending limb of the medulla in the kidney<sup>24</sup>; some scRNA-seq data have confirmed that *PPARA* is mainly expressed in proximal tubule cells in the kidney<sup>28,29</sup> (KIT Kidney Interactive Transcriptomics: <https://humphreyslab.com/SingleCell/>). Indeed, in this study, in the podocyte clusters (CL0) and distal tubule clusters (CL5) identified by scRNA-seq, there were no significant differences in the expression of PT maturation marker genes between the control and the PPAR $\alpha$  agonist conditions. These findings suggest that PPAR $\alpha$  pathway may not be involved in regulating the maturation rate of podocytes and distal tubules.

Cisplatin nephrotoxicity was evaluated in kidney organoids using conditions in which long-term treatment with low-dose cisplatin causes cell death, specifically in proximal tubules<sup>21</sup>. Cisplatin is taken up by proximal tubule cells by transporters expressed on the basolateral plasma membrane, such as *SLC22A2/OCT2* and *SLC31A1/CTR1*, and by megalin-mediated endocytosis, which leads to apoptosis<sup>30</sup>. Flow cytometry results showed that

the percentage of proximal tubule cells was reduced by cisplatin treatment. *SLC22A2* and *SLC31A1* gene expression levels tended to be higher in the PPAR $\alpha$  agonists-treated group than in the control group, but no significant difference in expression was observed (Supplementary Fig. 3a). Taken together, it is unlikely that cell death increased due to the increased uptake via these transporters, but future studies are needed to confirm the protein levels of these transporters. Regarding cisplatin uptake, it has been reported that it is taken up by endocytosis via *LRP2*<sup>31</sup>. In the present study, gene expression and protein level of *LRP2* were significantly increased in the PPAR $\alpha$  agonists-treated group, and the results of TEM and dextran uptake studies have shown increased uptake by endocytosis, indicating that the increased sensitivity to cisplatin is due to the increased uptake of cisplatin by endocytosis via *LRP2*. To test the possibility that the increased uptake of cisplatin by endocytosis results in increased cell death, experiments with drugs that inhibit endocytosis might be considered.

In this study, although the difference in the expression of maturation genes in proximal tubules of PPAR $\alpha$  agonists-treated kidney organoids was statistically significant, the level of maturation was found to be close to that of proximal tubules in fetuses around 11–18 weeks of gestation and did not reach the maturation level of child or adult proximal tubules (Fig. 4e). The likely reason for this is that the nine-day treatment period with the PPAR $\alpha$  agonist, intended to promote proximal tubule maturation, resulted in limited maturation. Considering the ten-month human gestation period, the duration of organoid culture may be insufficient to advance maturation to a child-like stage.

Regarding the batch effect, although strong batch effects have been reported in kidney organoids<sup>13</sup>, the current study was performed across different batches, and a significant increase in the maturation markers of proximal tubules was observed ( $n = 5-7$ ). This suggests that the acceleration of maturation rate by PPAR $\alpha$  agonist treatment is a universal response, irrespective of inter-batch differences.

Based on the above, to generate kidney organoids with a higher degree of proximal tubule maturation, a combination of multiple methodologies such as a method in the current study, long-term culture methods and differentiation techniques to improve early patterning of the nephrogenic mesenchyme<sup>32</sup>.

In summary, our time-course scRNA-seq analysis of the differentiation process of kidney organoids revealed that activation of the PPAR $\alpha$  pathway during differentiation induction can promote the maturation rate of proximal tubule cells. This, in turn, leads to increased gene expression levels in proximal tubule cells, functional maturation, and potentially enhanced susceptibility to cisplatin-induced nephrotoxicity. In the future, proximal tubule cells with an increased maturation rate by this approach could be used as cells in Microphysiological System (MPS) for further toxicity assessment and human extrapolation studies. Thus, the analysis of cell heterogeneity of the maturation rate within organoids indicates that it is possible to develop techniques to enhance organoid maturation. In the future, similar techniques to enhance the maturation rate of various organoids may be used more effectively for drug screening, regenerative medicine and other applications.

## Methods

### hiPSC culture and the differentiation of kidney organoids

Kidney organoids were generated from the hiPSC line CRL1502.C32 according to our previously published protocol<sup>33</sup> with some modifications (Fig. 1a). Briefly, hiPSCs were treated with 8  $\mu$ M CHIR99021 (TOCRIS, 4423) in APEL2 (StemCell Technologies, ST-05275) supplemented with 1% Protein Free Hybridoma Medium II (PFHM II, GIBCO, 12040077) (basal medium) for 5 days, followed by treatment with FGF9 (200 ng/mL, R&D, 273-F9) and heparin (1  $\mu$ g/mL, Sigma, H4784) for another 3 days. The cells were then collected and dissociated into single cells using TryPLE select (GIBCO, 12563011);  $1 \times 10^5$  collected cells were seeded into PrimeSurface<sup>®</sup> 96M plates (Sumitomo Bakelite) and were cultivated for 1 day in a CO<sub>2</sub> incubator to make spheroids. On the following day, these spheroids were transferred onto transwells with a 0.4  $\mu$ m pore polyester membrane

(Corning, 3450) and cultured at the liquid-air interface. Spheroids were treated with 10  $\mu$ M CHIR99021 in basal medium for 3 h and then cultured with FGF9 (200 ng/mL) and heparin (1  $\mu$ g/mL) for another 6 days, followed by another 16 days in basal medium with changing the medium every other day. For the PPAR $\alpha$  agonist or antagonist treatment, kidney organoids were treated with 0.3  $\mu$ M CP775146 (PPAR $\alpha$  agonist, TOCRIS, 4190) and 1  $\mu$ M 9-cis-retinoic acid (RXR $\alpha$  agonist, Abcam, ab141023) as agonist treatment group or 3 or 10  $\mu$ M GW6471 (PPAR $\alpha$  antagonist, TOCRIS, 4618) and 1 or 10  $\mu$ M HX531 (RXR antagonist, TOCRIS, 3912) as antagonists from day 15 in basal medium with medium change performed every other day.

### Single-cell isolation from kidney organoids

For preparing single cells from kidney organoids at days 15, 19, 23, 27 and 31 after the induction of differentiation, experiments were performed using 30–36 organoids from the same experimental run (36 organoids on day 15, 30 organoids on all other days). Kidney organoids were incubated for 30 min at 6 °C in cold active protease (DPBS(+), 5 mg/mL Bacillus Licheniformis Protease (Sigma, P5380), 125 U/mL DNase (Roche, 11284932001)<sup>34</sup> with pipetting 30 times every 5 min. Each cell suspension was diluted with fluorescence-activated cell sorting (FACS) buffer (DPBS(–), 0.5% FBS, 2 mM EDTA) + 125 U/mL DNase, centrifuged at 300 $\times$ g for 10 min at 4 °C after which the supernatant was removed. This step was repeated twice, after which the suspension was passed through a 35  $\mu$ m filtered tube (Falcon) to prepare a cell suspension containing single cells. Dead cells and Doublets were removed from these cells by BD FACSAria™ II & III using an Annexin V-FITC Apoptosis Detection Kit (Nakalai, 15342-54).

### Library preparation, sequencing and data pre-processing

Cell suspensions were adjusted to 1000 cells/ $\mu$ L, and libraries were prepared using Chromium Single Cell 3' reagent Kits (V3) according to the manufacturer's instructions. Libraries were sequenced using an Illumina NovaSeq 6000 Sequencing system with an average depth of 60,653 reads per cell, then mapped to the human genome (build GRCh38) and demultiplexed using Cell Ranger pipelines (10X Genomics, v.3.0.2). After performing a cellranger count for each sample, all samples were aggregated with cellranger aggr to create a gene expression matrix.

### Data processing and cell clustering

Pre-processed data from samples were further processed and analyzed individually using the R package Seurat (v.3.1.1) on RStudio (v.3.6.1)<sup>35</sup>. Clustering was performed using Seurat. For quality control of the data, UMI counts of cells, mitochondrial gene detection rate, and gene detection rates were prepared in violin plots, and then nCount\_RNA > 5000, percent.mt < 30, nFeature\_RNA < 7500 were filtered. The number of reads per droplet was then aligned to 10000 and normalized on a log scale. For clustering analysis, 2000 highly variable genes were extracted using the variance in expression levels and were Z-scored per gene using data from the entire sample. Notably, gene dependence on UMI counts, mitochondrial gene detection rate, S-phase score and G2M-phase score were corrected. PCA was performed using the Z-scored expression levels, and from JackStraw-Plots and ElbowPlots, the number of principal components for clustering was set to the top 20 and the resolution to 0.4. Cell types were identified by examining the expression of marker genes and cluster-specific genes of putative cell types.

### Sub-clustering

To identify detailed cell types that could not be classified by the parameters used for the whole sample, sub-clustering was performed for clusters (hereafter CL) 2, CL12, CL13 (NPC/PTA), CL4, CL5, CL9 (Tubules), and CL0, 1, 7 (Glomeruli). Clustering analysis was performed in the same way as the method for clustering all cells described above after extracting the clusters of interest, normalization, extraction of high variation genes, calculation of cell cycle score, Z-scoring, PCA, selection of a number of principal components, clustering, extraction of marker genes and cluster-specific genes, and annotation was performed for the sub-clusters.

### Pseudotime cell trajectory in kidney lineage cells

Samples of kidney cell lineages CL2, CL12, CL13 (NPC/PTA), CL4, CL5, CL9 (Tubules), and CL0, 1, 7 (Glomeruli) were extracted and differentiation trajectories were calculated using Monocle2 (ver.2.14.0)<sup>36</sup>. Using the extracted cells, PCA was performed on 1624 genes with large variance, and the top 10 principal components were used to compress the data into 2 dimensions using tSNE. Using tSNE density and peak data, clustering was performed with rho > 100 and delta > 15, which resulted in 8 clusters. Specific genes were detected among the clusters and a Pseudotime cell trajectory plot was created using 2021 genes with q-values of 0. To check whether the genes were aligned on the differentiation axis, a branched heatmap was created using known marker genes.

### Pseudotime cell trajectory in PT cells

Cells in the PT state of the pseudotime cell trajectory (PT cells in Fig. 2b) and cells annotated in the developmental lineage of the proximal tubule by UMAP sub-clustering (Supplementary Fig. 1f: cells in RV, Medial SSB, PT1 and PT2 clusters) were extracted. These cells were analyzed similarly to the analysis of pseudotime cell trajectory in kidney lineage cells to detect specific genes, and the top 320 genes with the lowest q-values were extracted. Pseudotime cell trajectory plots were created excluding mitochondrial genes and ribosomal protein-coding genes from the 320 genes. Maturation markers were obtained by extracting DEGs from the latter part of the pseudotime cell trajectory plot (Pseudotime 14–19) and other cells and selecting those that were more highly expressed in proximal tubule cells.

### DEG analysis and IPA analysis

DEGs were extracted using Seurat's function FindMarkers, using Poisson's method. Upstream regulators were analyzed by Ingenuity Pathway Analysis (IPA, Qiagen) using DEGs extracted by the above method.

### Isolation of LTL-positive cells from kidney organoids

LTL-biotin conjugated (Vector Laboratories, B-1325-2, 1:50) was added to the prepared single cell suspension and incubated at 4 °C for 15 min. The samples were then centrifuged at 300 $\times$ g for 5 min at 4 °C, and the supernatant was removed. The pellet was washed twice with FACS buffer. Anti-biotin micro Beads Ultra Pure (Miltenyi) were then added and incubated at 4 °C for 15 min, after which the samples were centrifuged at 300 $\times$ g for 5 min at 4 °C and the supernatant was removed. The pellet was washed twice with FACS buffer. The cell suspension was purified by the MACS method using an MS column (Miltenyi) fixed in a magnetic field to obtain LTL-positive cells.

### qPCR and heatmap

Total RNA was extracted from the LTL-positive proximal tubule cells obtained using a Purelink RNA micro kit (ThermoFisher Scientific). The total RNA obtained was used as a template for cDNA synthesis using Prime Script RT master mix (Perfect Real Time) (TaKaRa). The synthesized cDNA was quantified by real-time PCR using TB Green Premix Ex Taq II (Tli RNaseH Plus) (TaKaRa) for expression analysis. The sequences of primers used for qRT-PCR are listed in Supplementary Table 1. Heatmaps were created using Heatmap2 in R packages, and the tree was analyzed using Ward's method.

### IF staining

Organoids were fixed with 4% paraformaldehyde in DPBS (–) for 30 min at 4 °C followed by 3 washes with DPBS (–). The organoids were then blocked with 10% donkey serum, 0.3% Triton X/DPBS (–) for 3 h at room temperature and incubated with primary antibodies overnight at 4 °C. After 5 washes with 0.3% Triton X/DPBS (–), secondary antibodies were incubated overnight at 4 °C. The following antibodies and dilutions were used: mouse anti-ECAD (1:300, 610181, BD Biosciences), sheep anti-NPHS1 (1:300, AF4269, R&D Systems), LTL-biotin-conjugated (1:300, B-1325, Vector Laboratories), rabbit anti-Megalin (1:300, ab76969, Abcam), mouse anti- $\gamma$ H2AX (1:100, DNA Damage Detection Kit  $\gamma$ H2AX Red, G266, Dojindo

Laboratories). Images were taken using a Zeiss LSM800 confocal microscope or CQ1 (Yokogawa). All immunofluorescence analyses were successfully repeated more than three times and representative images are shown.

### Quantification of megalin fluorescence intensity

Fluorescence imaging of stained kidney organoids was performed using a Zeiss LSM800 confocal microscope. Z-stack images were acquired with a 10x objective at 3.4  $\mu\text{m}$  intervals. Maximum intensity projection (MIP) was applied to both megalin and DAPI fluorescence channels to generate 2D images from the 3D datasets. Megalin-positive areas and fluorescence intensities were quantified from the MIP images using Fiji software. Megalin fluorescence intensity per unit area was calculated by dividing the total megalin fluorescence intensity by the corresponding megalin-positive area. These values were then normalized to the average intensity of the day 20 control group, which was set as a baseline value of 1.

### scRNA-seq analysis of PPAR $\alpha$ agonist-treated kidney organoid samples

Kidney organoids were differentiated according to the previously described protocol until day 15. From day 15 to day 23, the control group was cultured in base medium supplemented with 0.2% DMSO, while the PPAR $\alpha$  agonists-treated group received base medium supplemented with 0.3  $\mu\text{M}$  CP775146 and 1  $\mu\text{M}$  9-cis-retinoic acid. ScRNA-seq data were generated as described for the time-course experiment. Libraries were sequenced on an Illumina NovaSeq 6000 system, yielding an average depth of 165,692 reads per cell. Quality control filtering was applied to retain cells with mitochondrial gene content <25% (percent.mt, <25) and gene counts between 2500 and 9500 (2500 < nFeature\_RNA < 9500). Control and PPAR $\alpha$  agonists-treated group datasets were integrated using the Seurat package's anchor-based CCA integration workflow (FindIntegrationAnchors and IntegrateData functions). Integrated expression data were Z-score normalized, and PCA was performed. Clustering was subsequently conducted using the top 20 principal components and a resolution of 0.2.

### Integration of kidney organoids and Kidney Cell Atlas (KCA) fetal kidneys

Cells annotated as "Cap mesenchyme," "Proliferating cap mesenchyme," "Proximal renal vesicle," "Distal renal vesicle," "Proliferating distal renal vesicle," "Proximal S-shaped body," "Medial S-shaped body," "Distal S-shaped body," "Proximal UB," "Podocyte," "Proximal tubule," "Loop of Henle," "Endothelium," "Stroma progenitor," and "Proliferating stroma progenitor" were extracted from the KCA fetal metadata, assuming their presence in the kidney organoids.

The KCA fetal data from six donors and two kidney organoid samples were integrated using Seurat's anchor-based CCA integration workflow (FindIntegrationAnchors and IntegrateData functions). Integrated expression data were Z-score normalized, and PCA was performed using the top 20 principal components for clustering with a resolution of 0.2.

### Pseudotime generation

Pseudotime was generated using the KCA metadata. Differentially expressed genes between proximal tubule and mSSB cell groups in the KCA fetal samples were identified (FindMarkers: logfc.threshold = 0.5, min.pct = 0.5, test.use = "poisson"). PT cells from KCA fetal cluster 4 (CL4) and three KCA child samples (Wilms1, Wilms2, Wilms3) were merged, and PCA was performed using the identified gene set.

### Pseudotime extrapolation

The generated pseudotime was used to extrapolate and compare the maturity of proximal tubules in organoids and adult kidneys. Pseudotime of organoid proximal tubule cells was calculated from the product of normalized expression in CL4 and the loading of the first principal component in the PCA.

Fetal kidney data for extrapolation was obtained from GSE114530. Proximal tubule cells (classified as CL4 using TransferData) were extracted, and pseudotime was calculated as described for organoids.

Adult kidney count data for extrapolation was obtained from GSE202109, with metadata from the UCSC Cell Browser. Proximal tubule cells were extracted, and pseudotime was calculated similarly.

### Transmission electron microscopy (TEM)

The tissue samples for TEM were fixed in phosphate-buffered 2% glutaraldehyde and subsequently post-fixed in 2% osmium tetra-oxide for 3 h in an ice bath. The specimens were then dehydrated in a graded ethanol series and embedded in epoxy resin. Ultrathin sections were obtained using an ultramicrotome. Ultrathin sections were stained with uranyl acetate for 10 min and a lead staining solution for 5 min and then observed by TEM (HITACHI H-7600 at 100 kV). The acquired images were used for quantification by Fiji to measure the area of the cytoplasm of the proximal tubule cells and the number and size of endosomes. As per the analysis, 24 images were used for the control group and 23 images for the PPAR $\alpha$  agonists-treated group, with 26 cells extracted from each.

### Dextran uptake assay

Kidney organoids on day 26 of differentiation cultured at the air-liquid interface in transwells were added to medium with pHrodo™ Red Dextran, 10,000 MW, for Endocytosis (Invitrogen, P10361) at 10 mg/mL and incubated at 37 °C in a 5% CO<sub>2</sub> incubator for 24 h. Organoids were then washed 3 times with ice-cold DPBS (–) and loaded into DPBS (–) containing LTL-FITC ((1:100) Vector Laboratories, FL-1321) for 2 h at 4 °C. Stained kidney organoids were observed for fluorescence using a CV8000 (Yokogawa). Images were taken with an X20 lens, and after acquiring 2 × 2 tiled images, images were taken every 5  $\mu\text{m}$  of 100  $\mu\text{m}$  thickness as a Z-stack. Average Intensity Projection (AveIP) was used for LTL fluorescence and Sum Intensity Projection (SumIP) was used for Dextran fluorescence to create 2D images from 3D images. Data analysis was performed using CellPathfinder (Yokogawa). The fluorescence intensity of dextran and LTL-positive region was measured. Then, the fluorescence intensity of dextran divided LTL-positive region. These values were then normalized to the average value of the control group, which was set as 1.

### Flow cytometry analysis of kidney organoids treatment with cisplatin

Kidney organoids on day 23 of differentiation were cultured for 6 days in medium containing 5  $\mu\text{M}$  cisplatin (cisplatin intravenous infusion 10 mg "Marco" (Nichi-Iko Pharma)). The medium was changed every other day. The kidney organoids were dissociated into single cells by the same method used for single-cell isolation from kidney organoids, and then the cells were suspended in 4% PFA/DPBS (–) and incubated at 37 °C for 10 min. The cells were then centrifuged at 300×g at 4 °C for 5 min, and the supernatant was removed. The cells were resuspended in 90% of cold methanol and incubated on ice for 30 min. The cells were resuspended in FACS buffer to make 10<sup>6</sup> cells/100  $\mu\text{L}$ . LTL-FITC (FL-1321, Vector Laboratories) was added at a concentration of 1:100, and the mixture was incubated for 30 min at 4 °C with a rotator. The cell suspension was centrifuged at 300×g at 4 °C for 5 min, the supernatant was removed and resuspended in FACS buffer and passed through a 35  $\mu\text{m}$  filtered tube (352235, Falcon). The cell suspensions were measured using a flow cytometer (NovoCyte, Agilent). The data were analyzed in Flowjo (Ver 10.6.2). The gating strategy for LTL-FITC was performed as follows: the population with the lowest fluorescence was gated to be negative, and all experiments were performed using the same gating. The gating strategy for FSC/SSC is shown in Supplementary Fig. 7.

### Quantification of $\gamma\text{H2AX}$ -positive cells in proximal tubules of kidney organoids treated with cisplatin

Stained kidney organoids were observed for fluorescence using a CQ1 (Yokogawa). Imaging was performed under the following conditions to

capture the entire organoid. Images were taken with an X10 lens, and after acquiring  $3 \times 3$  tiled images, images were taken every  $10 \mu\text{m}$  as a Z-stack. Maximum intensity projection (MIP) was applied to LTL,  $\gamma\text{H2AX}$  and DAPI fluorescence channels to generate 2D images from the 3D datasets. Data analysis was performed using CellPathfinder (Yokogawa), and the number of  $\gamma\text{H2AX}$ -positive cells was calculated by dividing the total number of  $\gamma\text{H2AX}$ -positive cells present within the LTL-positive region of the organoid by the total area ( $\mu\text{m}^2$ ) of the LTL-positive region. These values were then normalized to the average value of the cisplatin-untreated group, which was set as 1.

### Statistics and reproducibility

Statistical significance was determined by the unpaired two-tailed Student's *t*-test, Welch's *t*-test or paired *t*-test using SAS software for Windows, release 9.4 (SAS Institute Japan Ltd.). The mean, standard error, and statistical analysis results are shown in Supplementary Data 2. The number of replicates is defined in each figure legend.

### Reporting summary

Further information on research design is available in the Nature Portfolio Reporting Summary linked to this article.

### Data availability

The scRNAseq data obtained in this study were deposited in the Gene Expression Omnibus along with their associated metadata (GSE263556). The source data behind the figures in the paper are available in Supplementary Data 2. All other data are available from the corresponding author upon reasonable request.

Received: 10 February 2023; Accepted: 14 October 2024;

Published online: 27 November 2024

### References

1. Takasato, M. et al. Kidney organoids from human iPSCs contain multiple lineages and model human nephrogenesis. *Nature* **526**, 564–568 (2015).
2. Gupta, N. et al. Modeling injury and repair in kidney organoids reveals that homologous recombination governs tubular intrinsic repair. *Sci. Transl. Med.* **14**, eabj4772 (2022).
3. Lemos, D. R. et al. Interleukin-1b activates a MYC-dependent metabolic switch in kidney stromal cells necessary for progressive tubulointerstitial fibrosis. *J. Am. Soc. Nephrol.* **29**, 1690–1705 (2018).
4. Shimizu, T. et al. A novel ADPKD model using kidney organoids derived from disease-specific human iPSCs. *Biochem. Biophys. Res. Commun.* **529**, 1186–1194 (2020).
5. Vishy, C. E. et al. Genetics of cystogenesis in base-edited human organoids reveal therapeutic strategies for polycystic kidney disease. *Cell Stem Cell* **31**, 537–553.e5 (2024).
6. Hirayama, R. et al. iPSC-derived type IV collagen  $\alpha 5$ -expressing kidney organoids model Alport syndrome. *Commun. Biol.* **6**, 1–11 (2023).
7. Ohmori, T. et al. Impaired NEPHRIN localization in kidney organoids derived from nephrotic patient iPSCs. *Sci. Rep.* **11**, 1–12 (2021).
8. Jansen, J. et al. Human pluripotent stem cell-derived kidney organoids for personalized congenital and idiopathic nephrotic syndrome modeling. *Development* **149**, dev200198 (2022).
9. Low, J. H. et al. Generation of human PSC-derived kidney organoids with patterned nephron segments and a de novo vascular network. *Cell Stem Cell* **25**, 373–387.e9 (2019).
10. Homan, K. A. et al. Flow-enhanced vascularization and maturation of kidney organoids in vitro. *Nat. Methods* **16**, 255–262 (2019).
11. Wu, H. et al. Comparative analysis and refinement of human PSC-derived kidney organoid differentiation with single-cell transcriptomics. *Cell Stem Cell* **23**, 869–881.e8 (2018).
12. Sander, V. et al. Protocol for large-scale production of kidney organoids from human pluripotent stem cells. *STAR Protoc.* **1**, 100150 (2020).
13. Phipson, B. et al. Evaluation of variability in human kidney organoids. *Nat. Methods* **16**, 79–87 (2019).
14. Combes, A. N., Zappia, L., Er, P. X., Oshlack, A. & Little, M. H. Single-cell analysis reveals congruence between kidney organoids and human fetal kidney. *Genome Med.* **11**, 3 (2019).
15. Menon, R. et al. Single-cell analysis of progenitor cell dynamics and lineage specification in the human fetal kidney. *Development* **145**, dev164038 (2018).
16. Lindström, N. O. et al. Progressive recruitment of mesenchymal progenitors reveals a time-dependent process of cell fate acquisition in mouse and human nephrogenesis. *Dev. Cell* **45**, 651–660.e4 (2018).
17. Stewart, B. J. et al. Spatiotemporal immune zonation of the human kidney. *Science* **365**, 1461–1466 (2019).
18. McEvoy, C. M. et al. Single-cell profiling of healthy human kidney reveals features of sex-based transcriptional programs and tissue-specific immunity. *Nat. Commun.* **13**, 1–18 (2022).
19. Okada, T. & Morikawa, Y. Development of the proximal tubule of the fetal rat kidney: morphometry and ultrastructural findings. *Ann. Anat.* **175**, 89–94 (1993).
20. Larsson, L. & Maunsbach, A. B. Differentiation of the vacuolar apparatus in cells of the developing proximal tubule in the rat kidney. *J. Ultrastruct. Res.* **53**, 254–270 (1975).
21. Digby, J. L. M., Vanichapol, T., Przepiorski, A., Davidson, A. J. & Sander, V. Evaluation of cisplatin-induced injury in human kidney organoids. *Am. J. Physiol. Renal Physiol.* **318**, F971–F978 (2020).
22. Morizane, R. et al. Nephron organoids derived from human pluripotent stem cells model kidney development and injury. *Nat. Biotechnol.* **33**, 1193–1200 (2015).
23. Ruan, X., Zheng, F. & Guan, Y. PPARs and the kidney in metabolic syndrome. *Am. J. Physiol. Renal Physiol.* **294**, 1032–1047 (2008).
24. Guan, Y., Zhang, Y., Davis, L. & Breyer, M. D. Expression of peroxisome proliferator-activated receptors in urinary tract of rabbits and humans. *Am. J. Physiol. Renal Physiol.* **273**, F1013–F1022 (1997).
25. Forbes, J. M. Mitochondria—power players in kidney function? *Trends Endocrinol. Metab.* **27**, 441–442 (2016).
26. Wang, G. et al. Spatial dynamic metabolomics identifies metabolic cell fate trajectories in human kidney differentiation. *Cell Stem Cell* **29**, 1580–1593.e7 (2022).
27. Dhillon, P. et al. The nuclear receptor ESRRA protects from kidney disease by coupling metabolism and differentiation. *Cell Metab.* **33**, 379–394.e8 (2021).
28. Wu, H. et al. Single-cell transcriptomics of a human kidney allograft biopsy specimen defines a diverse inflammatory response. *J. Am. Soc. Nephrol.* **29**, 2069–2080 (2018).
29. Muto, Y. et al. Single cell transcriptional and chromatin accessibility profiling redefine cellular heterogeneity in the adult human kidney. *Nat. Commun.* **12**, 2190 (2021).
30. Pabla, N. & Dong, Z. Cisplatin nephrotoxicity: mechanisms and renoprotective strategies. *Kidney Int.* **73**, 994–1007 (2008).
31. Hori, Y. et al. Megalin blockade with cilastatin suppresses drug-induced nephrotoxicity. *J. Am. Soc. Nephrol.* **28**, 1783–1791 (2017).
32. Vanslambrouck, J. M. et al. Enhanced metanephric specification to functional proximal tubule enables toxicity screening and infectious disease modelling in kidney organoids. *Nat. Commun.* **13**, 5943 (2022).
33. Takasato, M., Er, P. X., Chiu, H. S. & Little, M. H. Generation of kidney organoids from human pluripotent stem cells. *Nat. Protoc.* **11**, 1681–1692 (2016).
34. Adam, M., Potter, A. S. & Potter, S. S. Psychrophilic proteases dramatically reduce single-cell RNA-seq artifacts: a molecular atlas of kidney development. *Development* **144**, 3625–3632 (2017).

35. Stuart, T. et al. Comprehensive integration of single-cell data. *Cell* **177**, 1888–1902.e21 (2019).
36. Trapnell, C. et al. The dynamics and regulators of cell fate decisions are revealed by pseudotemporal ordering of single cells. *Nat. Biotechnol.* **32**, 381–386 (2014).

### Acknowledgements

We thank S. Kuraku, M. Kadota and O. Nishimura for assistance with scRNA-seq library preparation and RNA sequencing and I. Nikaïdo for assistance with data analysis of scRNA-seq. This work was supported by the RIKEN BDR-Otsuka Pharmaceutical Collaboration Center (RBOC), JSPS KAKENHI Grant Numbers JP18H05108, and AMED Grant Numbers JP17be0304205, JP17be0304321, and JP22be1004204.

### Author contributions

Y.S. and M.T. conceived and designed experiments and wrote the manuscript; Y.S. and C.F. performed experiments; Y.S. and Y.K. analyzed the single-cell RNA-seq data; M.T. supervised the project; all authors reviewed and edited the manuscript.

### Competing interests

The authors declare no competing interests.

### Additional information

**Supplementary information** The online version contains supplementary material available at <https://doi.org/10.1038/s42003-024-07069-6>.

**Correspondence** and requests for materials should be addressed to Minoru Takasato.

**Peer review information** *Communications Biology* thanks Ryuji Morizane, Veronika Sander, and the other anonymous reviewers for their contribution to the peer review of this work. Primary handling editors: Rosie Bunton-Stasyshyn and Anam Akhtar.

**Reprints and permissions information** is available at <http://www.nature.com/reprints>**Publisher's Note** Springer Nature remains neutral with regard to jurisdictional claims in published maps and institutional affiliations.

**Open Access** This article is licensed under a Creative Commons Attribution-NonCommercial-NoDerivatives 4.0 International License, which permits any non-commercial use, sharing, distribution and reproduction in any medium or format, as long as you give appropriate credit to the original author(s) and the source, provide a link to the Creative Commons licence, and indicate if you modified the licensed material. You do not have permission under this licence to share adapted material derived from this article or parts of it. The images or other third party material in this article are included in the article's Creative Commons licence, unless indicated otherwise in a credit line to the material. If material is not included in the article's Creative Commons licence and your intended use is not permitted by statutory regulation or exceeds the permitted use, you will need to obtain permission directly from the copyright holder. To view a copy of this licence, visit <http://creativecommons.org/licenses/by-nc-nd/4.0/>.

© The Author(s) 2024